ACS APPLIED MATERIALS & INTERFACES

www.acsami.org
Research Article

Harnessing RNA Technology to Advance Therapeutic Vaccine Antigens against Chagas Disease

Chiara Mancino, Jeroen Pollet, Assaf Zinger,* Kathryn M. Jones, Maria José Villar, Ana Carolina Leao, Rakesh Adhikari, Leroy Versteeg, Rakhi Tyagi Kundu, Ulrich Strych, Federica Giordano, Peter J. Hotez, Maria Elena Bottazzi, Francesca Taraballi,* and Cristina Poveda*

Cite This: *ACS Appl. Mater. Interfaces* 2024, 16, 15832−15846
Read Online

ACCESS | Metrics & More | Article Recommendations | Supporting Information

ABSTRACT: Chagas disease (CD) (American trypanosomiasis caused by *Trypanosoma cruzi*) is a parasitic disease endemic in 21 countries in South America, with increasing global spread. When administered late in the infection, the current antiparasitic drugs do not prevent the onset of cardiac illness leading to chronic Chagasic cardiomyopathy. Therefore, new therapeutic vaccines or immunotherapies are under development using multiple platforms. In this study, we assessed the feasibility of developing an mRNA-based therapeutic CD vaccine targeting two known *T. cruzi* vaccine antigens (Tc24—a flagellar antigen and ASP-2—an amastigote antigen). We present the mRNA engineering steps, preparation, and stability of the lipid nanoparticles and evaluation of their uptake by dendritic cells, as well as their biodistribution in c57BL/J mice. Furthermore, we assessed the immunogenicity and efficacy of two mRNA-based candidates as monovalent and bivalent vaccine strategies using an in vivo chronic mouse model of CD. Our results show several therapeutic benefits, including reductions in parasite burdens and cardiac inflammation, with each mRNA antigen, especially with the mRNA encoding Tc24, and Tc24 in combination with ASP-2. Therefore, our findings demonstrate the potential of mRNA-based vaccines as a therapeutic option for CD and highlight the opportunities for developing multivalent vaccines using this approach.

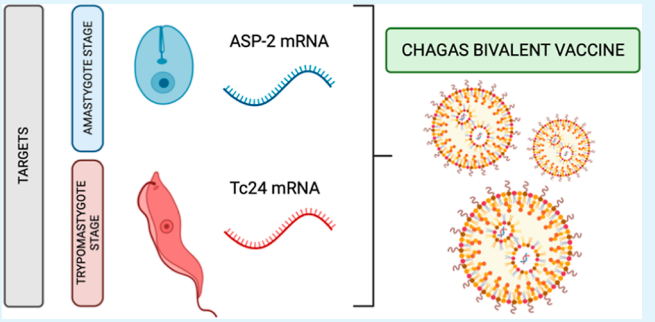

KEYWORDS: *Chagas disease, mRNA vaccine, lipid nanoparticles, biodistribution, immunogenicity*

INTRODUCTION

The neglected tropical disease known as Chagas disease (CD) arises after infection with the flagellated protozoan parasite *Trypanosoma cruzi* (*T. cruzi*).[1] Now endemic in 21 countries in the Americas, CD accounts for ∼56,000 new infections yearly, a total of nearly 6−7 million infected individuals.[2−4] It is now spreading to nonendemic countries due to globalization.[3] Worldwide estimates show how CD accounts for about 10,000 deaths and 800,000 "Disability Adjusted Life Years" (DALYs) annually.[5]

T. cruzi is transmitted principally via a triatomine vector, although it can also spread via oral transmission, as well as through organ transplants, contaminated food sources, blood transfusions, and congenitally.[6] CD starts with a short acute phase characterized by high proliferation of *T. cruzi*.[1,7] Following this acute phase, parasitemia subsides during the chronic phase, leaving most patients asymptomatic even though patients remain seropositive to *T. cruzi* antigens and *T. cruzi* DNA can be detected in their blood by polymerase chain reaction. Such patients are presumed to maintain the infection, and they are clinically recognized as having what is commonly referred to as an "indeterminate status". Unfortunately, 30−40% of infected and indeterminate patients will progress to cardiac and gastrointestinal complications (determinate CD) between 10 to 30 years postacute phase, with the worst cases leading to death.[3,8] Available treatment strategies rely on two main drugs, nifurtimox and benznidazole, whose benefits are significant only when intervention occurs during the early stages of infection.[3] Moreover, their efficacy is tied to a lengthy treatment regimen (up to 60 days), during which patients experience many side effects that often lead to patients dropping the treatment regimen. Therefore, there is currently little to offer to determine patients who are diagnosed late in their illness, especially individuals showing signs and symptoms of chronic Chagasic cardiomyopathy (CCC). CCC is characterized by the presence of arrythmias, cardiac aneurysms, and heart failure as well as

Received: December 15, 2023
Revised: February 29, 2024
Accepted: March 1, 2024
Published: March 22, 2024

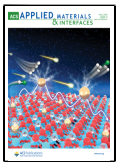

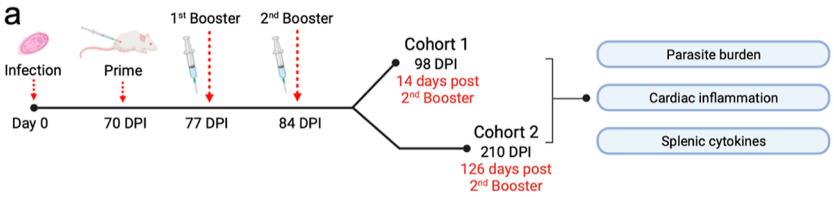

b

Treatment group	Antigen dose
Saline	-
Empty LNPs	-
Tc24 mRNA LNPs	10 μg
ASP-2 mRNA LNPs	10 μg
Tc24+ASP-2 mRNA LNPs	10 μg each antigen

Figure 1. mRNA-based therapeutic Chagas vaccine. (a) Timeline of the therapeutic vaccination strategy. Mice were infected with 500 blood-form trypomastigotes of *T. cruzi* H1 clone K68 by intraperitoneal injection. All of the mice received three immunizations subcutaneously a week apart (70, 77, and 84 DPI). The initial evaluation was 2 weeks after the final vaccination at 98 DPI [14 days post booster (DPB), 5 mice per group] and the final evaluation at day 210 DPI (126 DPB, 10 mice per group). The mice were humanely euthanized, and their blood, heart, and skeletal muscle were collected for parasitological evaluation; spleens were collected to measure antigen-specific immune response. (b) Experimental groups and antigen doses.

strokes and other complications. Through these mechanisms, CCC is an important cause of mortality in disease-endemic regions.

For such chronically infected CD patients, efforts to develop a therapeutic vaccine are ongoing, with the potential of use as an immunotherapy to delay or prevent cardiac complications in patients with chronic *T. cruzi* infection.[9] Different vaccine strategies have been evaluated through animal models of CD, ranging from traditional approaches using live attenuated parasites, recombinant proteins formulated with adjuvants and immunostimulants, genetic vaccinations, and the delivery of DNA via different vectors.[1,3] However, one of the main challenges for a successful CD vaccine development strategy is the selection of the target antigen, which ideally should demonstrate immunogenicity and efficacy across different parasite strains or developmental life-history stages.[1,3] For example, targeting the infective metacyclic trypomastigote, transferred from vector to host, could potentially prevent parasitemia development, causing sterile immunity. However, this parasite stage is highly specialized in its immune system evasion thanks to the ability of antigen diversification as the mechanism used by the parasite for host cell invasion.[7,10] Therefore, targeting the later stages of *T. cruzi*, such as the intracellular amastigote and extracellular trypomastigote forms, could also help control parasitemia in later stages of infection, leading to improved patient outcome.

In this context, two well-explored antigens, the amastigote surface antigen 2 (ASP-2) and the flagellar calcium-binding flagellar protein Tc24 (highly expressed in the trypomastigote stage), present a unique opportunity to evaluate them alone or in combination by utilizing mRNA-based vaccine technology. Both antigens have been evaluated as DNA or recombinant protein antigens in a variety of preclinical animal models, including mice, dogs, and even nonhuman primates.[1,3,7,8] They were shown to stimulate the $CD4^+$-mediated production of Interferon-γ (IFN-γ), as well as activation of cytotoxic T cells ($CD8^+$). Specifically, it has been shown that recombinant ASP-2 associated with CpG oligodeoxynucleotides or alum elicited a strong $CD8^+$ T cell response, subsequently leading to protective immunity in mice.[11] In addition, recombinant Tc24 used in association with MPLA (monophosphoryl-lipid A) or other Toll-like receptor 4 adjuvants, including glucopyranosyl lipid A or E6020, resulted in a balanced Th1/Th2 response with increased levels of IFN-γ in mice.[9,12] Accordingly, a recombinant Tc24-based therapeutic CD vaccine is under development and advancing to human trials.[9] As an alternative or as a complementary approach to administering recombinant protein-based CD vaccines, DNA for these antigens was also explored, being delivered to the cell's nuclei either naked, via plasmids, or using a wide variety of viral vectors.[13−17] With the global successes in administering mRNA (mRNA) vaccines for COVID-19, new opportunities are available to accelerate product and clinical development for other infectious diseases. Researchers have already recognized the potential of mRNA-based vaccines in addressing challenges associated with traditional vaccine development for CD.[18,19]

In this study, we assessed the feasibility of developing an mRNA-based therapeutic CD vaccine targeting two *T. cruzi* vaccine antigens (Tc24 and ASP-2). The most widespread approach for mRNA delivery relies on nanomedicine: lipid nanoparticles (LNPs) are lipid-based vesicles that can be loaded with mRNA payloads.[20] LNPs are usually administered intramuscularly, where they are taken up by antigen-presenting cells (APCs) [primarily dendritic cells (DCs)]: LNPs release the mRNA cargo in the cytoplasm and trigger protein translation, leading to the production of functional antigens that resemble those presented by pathogens during a natural infection to the immune system, thus mimicking the mechanism of natural infection.[21] Here, we outlined the mRNA synthesis process and the preparation and stability assessment of the LNPs, and examined their uptake by DCs, as well as their biodistribution in C57BL/J mice. Furthermore, we comprehensively assessed the mRNA-based monovalent and bivalent vaccines by measuring their impact on early cardiac damage caused by *T. cruzi* infection, effects on parasite burden, and vaccine-specific immune response (as summarized in Figure 1a,b). With this work, we evaluated the concept of delivering multiple mRNA antigens within the same LNP delivery system for CD. Bivalent

https://doi.org/10.1021/acsami.3c18830
ACS Appl. Mater. Interfaces 2024, 16, 15832−15846

vaccination can offer several advantages by enhancing protection against different stages of pathogens, potentially providing more robust responses.

RESULTS AND DISCUSSION

LNPs Loaded with Tc24, ASP-2, and Tc24 + ASP-2 mRNA Are Homogeneous and Stable. LNPs containing the mRNA encoding Tc24, ASP-2, and Tc24 in combination with ASP-2 were synthesized using the microfluidic system benchtop NanoAssemblr, which exploits a microfluidic cartridge that mixes an organic phase, usually containing lipids dissolved in ethanol, and an aqueous phase, containing the synthesis buffer alongside the cargo.[22,23] LNPs were synthesized with the ionizable lipid known as DLin-MC3-DMA, previously approved by the FDA to deliver siRNA. Briefly, an N/P ratio (quaternary nitrogen of DLin-MC3-DMA/phosphate of mRNA) of 5.6 allowed for successful complexation of the ionizable lipid with the following mRNA constructs: (i) Tc24 mRNA, (ii) ASP-2 mRNA, and (iii) a combination of Tc24 and ASP-2 mRNA (1:1 w/w ratio). Empty LNPs were used as the control. The stability of the physio-chemical properties of LNPs was evaluated with dynamic light scattering (DLS) for up to 28 days upon storage at 4 °C.

The average LNP size was around ∼100 nm independently of the construct used (80.13 ± 8.12 nm for empty LNPs, 91.27 ± 0.51 nm for Tc24 LNPs, 86.96 ± 3.84 nm for ASP-2 LNPs, and 81.6 ± 9.45 nm for Tc24 + ASP-2 LNPs, as shown in Figure 2a), and it was maintained stable for up to a month after synthesis. Size distribution was homogeneous and consistent over time, as indicated by the low polydispersity indexes (PDIs <0.2, Figure 2b). Finally, the surface charge of LNPs was always negative, with a slight decrease of zeta potential (ZP) over time for loaded LNPs (from −3.34 ± 1.91 mV to −8.43 ± 1.83 mV for Tc24 LNPs, from −2.73 ± 1.3 mV to −9.52 ± 0.54 mV for ASP-2 LNPs, and from −4.27 ± 0.89 mV to −8.87 ± 0.62 mV for Tc24 + ASP-2 LNPs, as shown in Figure 2c), which is hypothesized to be related to a rearrangement of the contents of the solid core of the LNPs, with the mRNA constructs moving closer to the surface of the LNPs. The encapsulation efficiency (EE %), evaluated with Ribogreen, revealed that over 75% of the genetic cargo was successfully encapsulated by our LNPs (Figure 2d). In detail, LNPs prepared with the Tc24 construct had the highest EE % (116.89 ± 12.80%), while only 86.88% ± 1.27% of the ASP-2 mRNA was successfully encapsulated. Consistently with these results, LNPs with the combination of the two constructs had an average EE %, accounting for the lower efficiency present for the ASP-2 construct (108.23 ± 8.27%). The size and presence or absence of the genetic cargo were confirmed by CryoTEM, as indicated by the electron-dense areas in the LNPs loaded with genetic cargo compared with empty LNPs (Figure 2e).

Notably, results show that all the LNPs were stable for up to 28 days postsynthesis when stored at 4 °C, indicating that the LNPs are a very robust system for storing genetic cargo. The stringent storage conditions, requiring ultralow temperatures (−20/-80 °C) for certain COVID-19 vaccines, pose significant logistical challenges, particularly in tropical countries.[24−26] Maintaining the cold chain demands specialized infrastructure, reliable transportation, and constant monitoring, which may be limited in regions with warmer climates. This difficulty in maintaining the required storage conditions can lead to delays and complexities in vaccine distribution, especially in remote or underserved areas. Moreover, the economic burden associated with establishing and sustaining the necessary cold chain infrastructure raises concerns about equity in vaccine access. To address these challenges, some countries have opted for vaccines with flexible storage requirements. Ongoing efforts are focused on innovations in storage technology, potentially leading to the development of vaccines that are not as reliant on ultralow temperatures. These advancements aim to enhance the accessibility and distribution of COVID-19 vaccines, ensuring that vaccination campaigns can effectively reach diverse populations worldwide. Hence, we evaluated the feasibility of maintaining our proposed mRNA vaccine under 4 °C storage, providing evidence of stability of physiochemical properties and mRNA integrity, despite some possible rearrangement of the cargo within the LNP structure indicated by the decrease in ZP. In fact, our observations are supported by the readouts over construct integrity obtained via Bioanalyzer (Figure 2f): both LNPs loaded with single constructs (either Tc24 or ASP-2) or their combination, successfully protected the mRNAs from degradation, as shown by the absence of bands at lower molecular weights than the ones corresponding to the constructs. Moreover, these agarose gels confirmed the presence of both constructs when LNPs were loaded with a combination of Tc24 and ASP-2, while fainter bands were observed for the ASP-2 construct, supporting our hypothesis for the lower EE % of this specific construct.

In Vitro Toxicity and Uptake. Prior to advancing to in vivo preclinical studies, it is essential to assess the safety and effectiveness of a formulation through in vitro evaluations.[27] These tests allowed us to identify any potential toxicity related to the formulation itself. In addition, it allows for a more cost-effective and rapid way to test for formulation efficacy preliminarily. Hence, given that the target cell type for mRNA-based vaccines is represented by DCs, we assessed the cytotoxicity of our delivery system (empty LNPs) in DCs at different lipidic concentrations (0, 12.5, 25, 50, and 100 μM) using a murine DC line. Results revealed a threshold of 50 μM (lipidic concentration) over which a significant drop in cell viability was observed only 40% of the cells survived at a 50 μM concentration, as shown in Figure 3a. Therefore, the 50 μM concentration was selected to evaluate the uptake of the LNPs by DCs after treatment with rhodamine labeled LNPs. Results revealed a 6-fold increase in uptake signal after 24 h of treatment (Figure 3b,c), confirming the ideal formulation to advance to in vivo studies. While the exact mechanisms of DC uptake of LNPs are still under investigation, our in vitro experiment with the DC2.4 cell line shows that this target cell type can successfully uptake the LNPs. This is of utmost importance for vaccine applications, where uptake of LNPs by APCs is the first step toward achieving immunity. Once internalized in endosomes, LNPs can be released in the cytoplasm thanks to the intrinsic physio-chemical properties of the ionizable lipid. The acidic pH of the endosome triggers the protonation of the ionizable lipid (DLin-MC3-DMA), which, in turn, interacts with the negatively charged lipids of the endosomal membrane, disrupting the LNP structure and causing the release of the genetic cargo in the cytoplasm, where it is available for protein translation.[28] Validation of the successful translation of the Tc24 antigen has been provided in our previous publication by Poveda et al., 2023, where Western Blotting has been used to measure Tc24 protein expression upon delivery of 1 μg of Tc24 mRNA to DCs through the same LNP formulation characterized here.[19]

In Vivo Toxicity and Biodistribution. Drug delivery systems for mRNA delivery aim at protecting the genetic cargo

https://doi.org/10.1021/acsami.3c18830
ACS Appl. Mater. Interfaces 2024, 16, 15832−15846

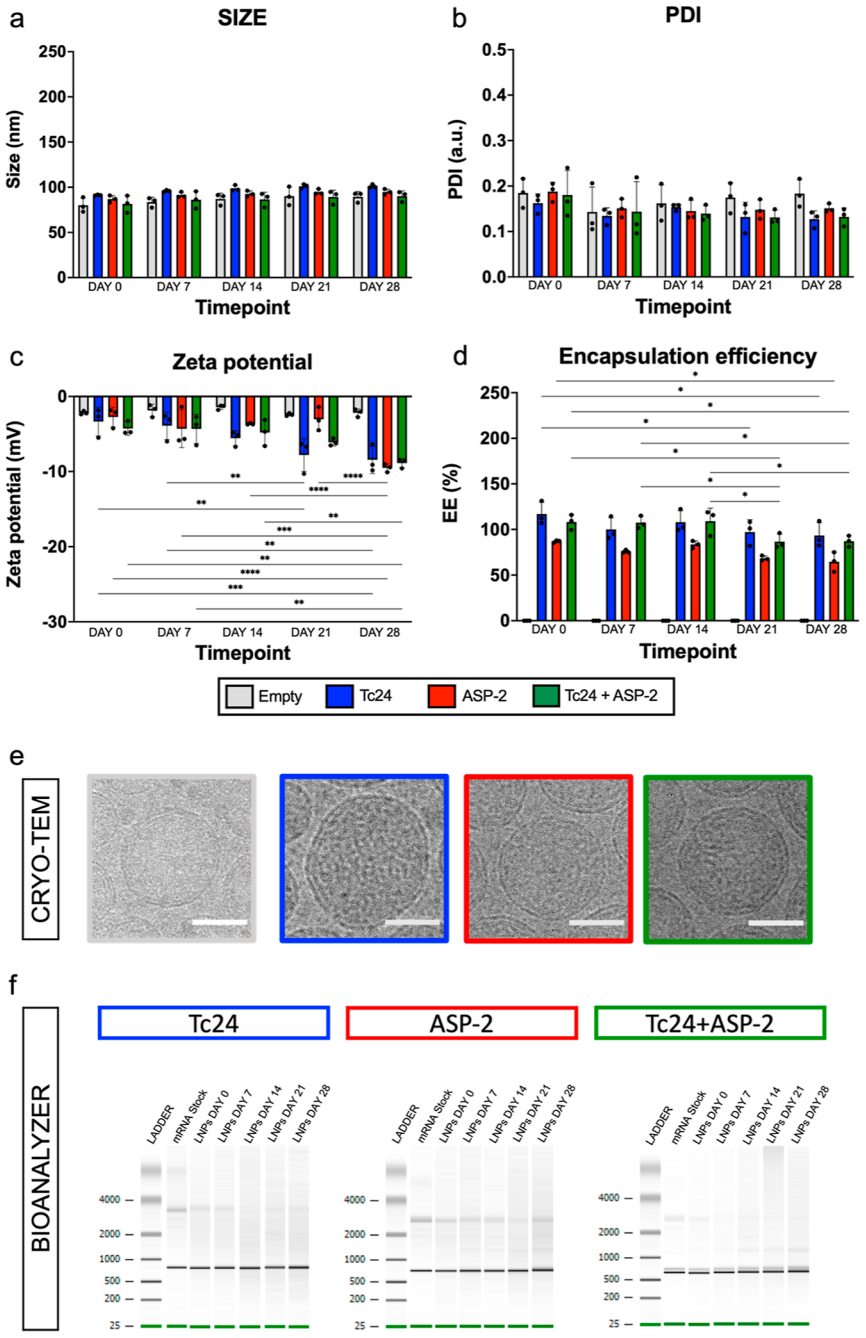

Figure 2. Physio-chemical properties and stability of LNPs. The stability of the physio-chemical properties of LNPs was evaluated with DLS for up to 28 days upon storage at 4 °C. (a) The size of the LNPs, approximately ∼100nm, remained consistent regardless of the construct used, and this size was maintained for up to one month after synthesis. (b) The size distribution of LNPs exhibited homogeneity and consistency over time, as evidenced by the low polydispersity indices (PDIs) (<0.2). (c) The LNPs consistently displayed a negative surface charge, with a slight decrease in ZP over time. (d) Ribogreen analysis revealed a high encapsulation efficiency (EE %) of over 75%, indicating successful encapsulation of the genetic cargo within the LNPs. (e) CryoTEM imaging confirmed the presence or absence of genetic cargo within the LNPs. Electron-dense areas were observed in LNPs loaded with genetic cargo, distinguishing them from empty LNPs. Scale bars of 100A were used for size determination. (f) Assessment of construct integrity via Bioanalyzer demonstrated that LNPs loaded with single constructs (either Tc24 or ASP-2) as well as their combination effectively protected the mRNAs from degradation. This was evident from the absence of bands corresponding to lower molecular weights than those of the constructs. Furthermore, agarose gel analysis confirmed the presence of both constructs when LNPs were loaded with a combination of Tc24 and ASP-2. *P*-values of ≤0.05, ≤0.01, ≤0.001, and ≤0.0001 are represented as one, two, three, and four symbol characters, respectively.

while ensuring lower construct immunogenicity and successful delivery of the cargo to target cells and tissues for protein expression.[29] Therefore, evaluating the LNP performance in vivo is essential, since different applications might require different administration routes. With this in mind, LNPs' toxicity and biodistribution were assessed in vivo in C57BL/6J mice using four different administration routes: (i) intravenous (IV), (ii) subcutaneous (SC), (iii) intramuscular (IM), and (iv) intraperitoneal (IP). In detail, mice were administered Luciferase mRNA loaded LNPs, so that two readouts could be

https://doi.org/10.1021/acsami.3c18830
ACS Appl. Mater. Interfaces 2024, 16, 15832−15846

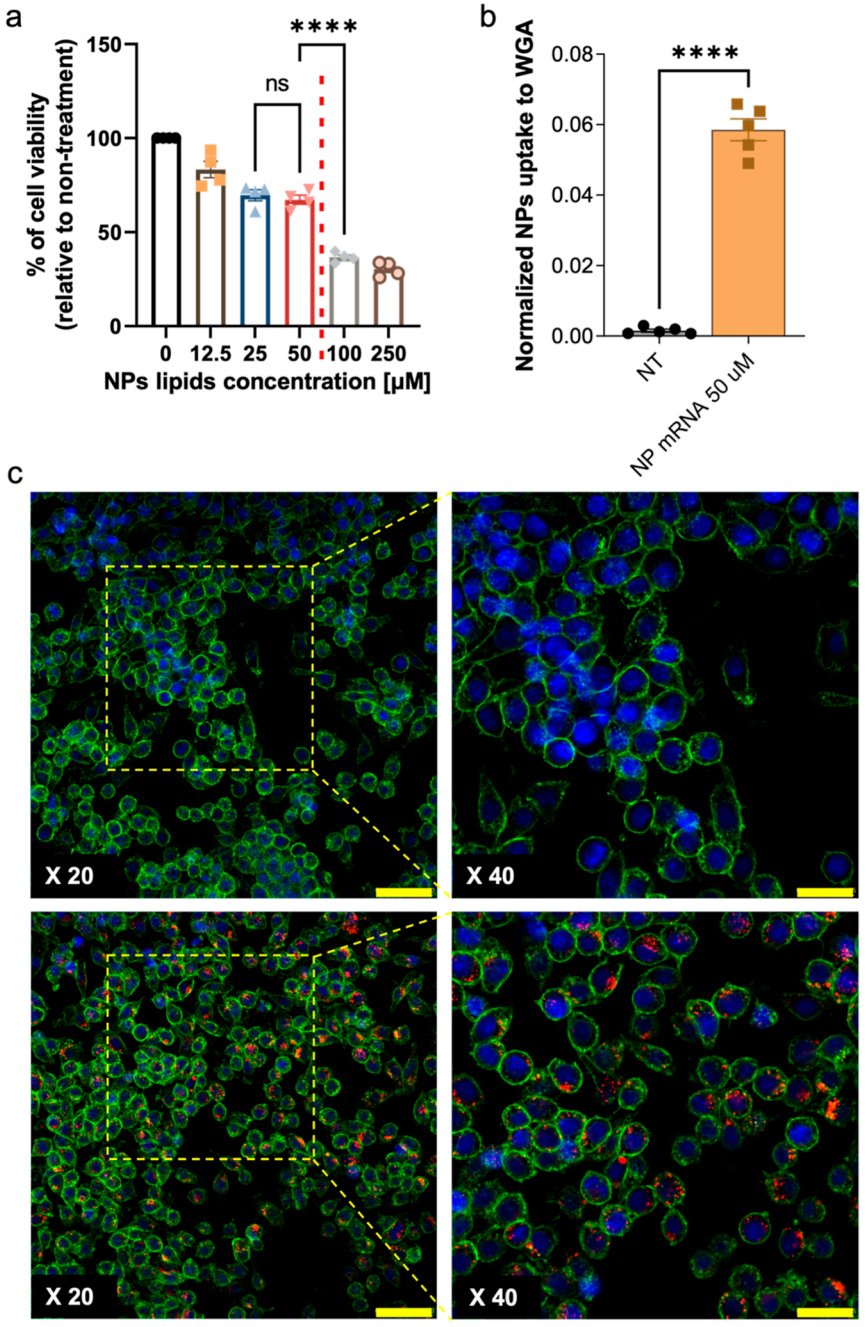

Figure 3. In vitro toxicity and uptake of LNPs. The cytotoxicity of empty LNPs was assessed in the DC2.4 murine cell line at varying concentrations of lipids. The findings are as follows: (a) the results indicated that a lipid concentration exceeding 50 μM crossed a threshold, resulting in a significant decrease in cell viability. (b) Once a safe dosage was determined, DCs were exposed to rhodamine-labeled LNPs to assess uptake [red color represents LNPs, green color corresponds to wheat germ agglutinin (WGA) representing the cytoskeleton, and nuclei are in blue—DAPI]. The results demonstrated a sixfold increase in the uptake signal after 24 h of treatment. (c) Representative images were captured to illustrate the uptake of LNPs by DCs. The top images depict untreated cells, while the bottom images display cells treated with LNPs. Images on the left were captured with 20× magnification (scalebar 50 μm), while pictures to the right were captured with a 40× magnification (scalebar 25 μm). *P*-values of ≤0.05, ≤0.01, ≤0.001, and ≤0.0001 are represented as one, two, three, and four symbol characters, respectively.

gathered from the experiment: fluorescently labeled LNPs allowed us to appreciate the biodistribution of nanoparticles in different organs (representative images in Figure 4a), while a luminescence signal was used to confirm the success of mRNA translation upon administration of the luciferase substrate (representative images in Figure 4b). Results from the fluorescence reading at 18 h postinjection showed significant differences in LNPs biodistribution for the four administration routes (Figure 4c). As expected for vesicles of ∼100 nm size, (i) IV administration revealed the highest accumulation in the liver ($1.12 \times 10^9 \pm 3.19 \times 10^8$ p/s/cm^2/sr), spleen ($5.33 \times 10^8 \pm 1.91 \times 10^8$ p/s/cm^2/sr), and lungs ($1.22 \times 10^8 \pm 2.43 \times 10^7$ p/s/cm^2/sr), respectively.[30] The highest protein expression (obtained from the luminescence signal arising from luciferase expression) was found in the same organs ($5.02 \times 10^6 \pm 1.53 \times 10^6$ p/s/cm^2/sr for liver, $1.31 \times 10^5 \pm 6.48 \times 10^4$ p/s/cm^2/sr for spleen, and $2.54 \times 10^4 \pm 8.44 \times 10^3$ p/s/cm^2/sr for lungs, Figure 4d). (ii) SC administration gave a minimal signal for

https://doi.org/10.1021/acsami.3c18830
ACS Appl. Mater. Interfaces 2024, 16, 15832−15846

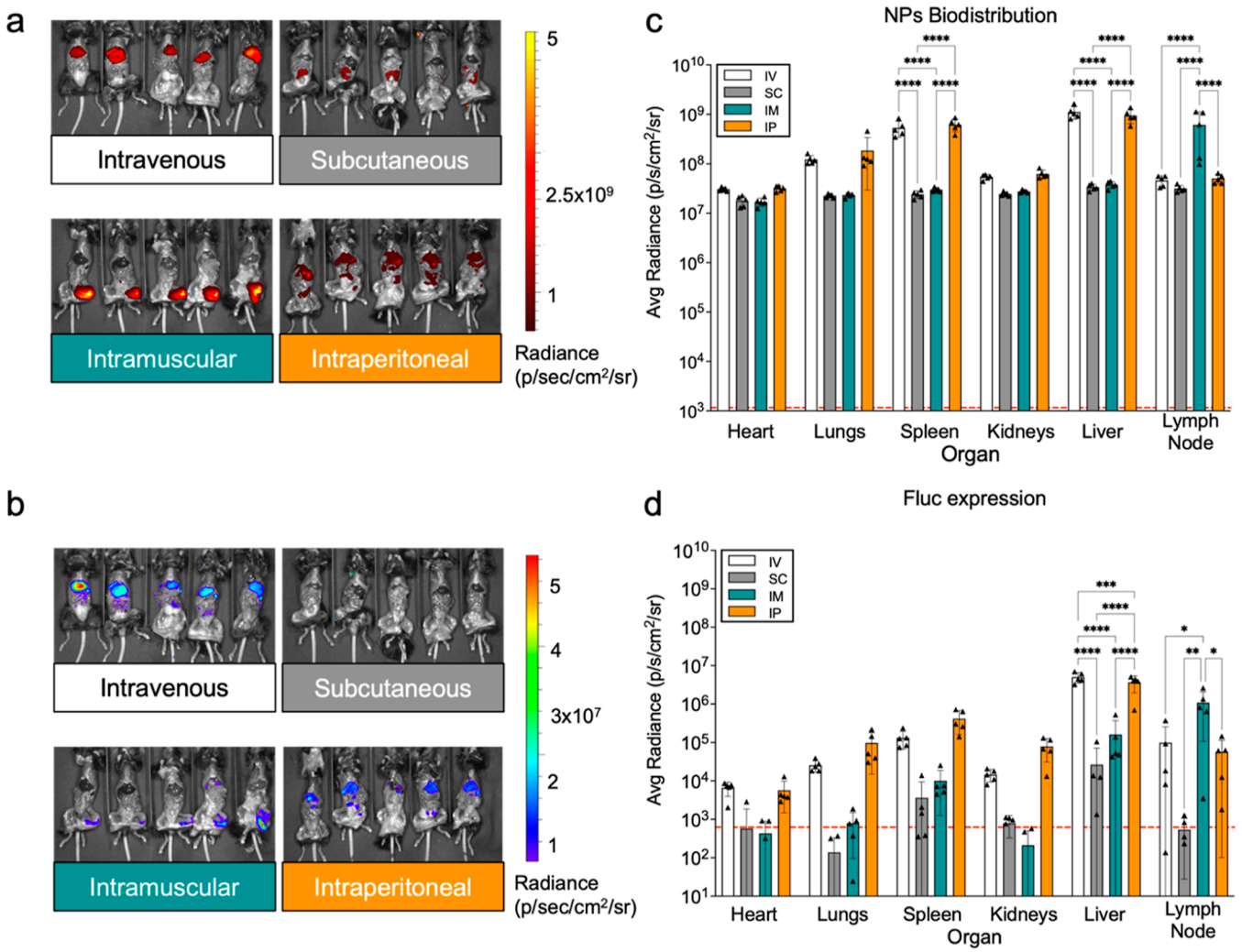

Figure 4. In vivo biodistribution of LNPs. The in vivo biodistribution of LNPs was investigated in C57BL/J mice, utilizing four distinct administration routes: (i) intravenous (IV), (ii) subcutaneous (SC), (iii) intramuscular (IM), and (iv) intraperitoneal (IP). The following key points summarize the findings: (a) representative images of in vivo biodistribution of fluorescently labeled LNPs. (b) Representative images were obtained to validate successful mRNA translation by assessing the luminescence signal upon administration of the luciferase substrate. In order to have an immediate visual readout of the signal from both the LNPs and the translated protein, the authors sacrificed the mice and exposed all internal organs for imaging before necropsy. (c) Biodistribution data analysis was conducted to compare the LNPs' signal across different administration routes (red dotted line represents background signal). (d) Quantification of luciferase protein translation was performed to compare the signal generated by different administration routes (red dotted line represents background signal). *P*-values of ≤0.05, ≤0.01, ≤0.001, and ≤0.0001 are represented as one, two, three, and four symbol characters, respectively.

fluorescence (the highest signal was present in the liver: $3.37 \times 10^7 \pm 4.98 \times 10^6$ p/s/cm^2/sr) and bioluminescence (the liver signal being $2.65 \times 10^4 \pm 4.43 \times 10^4$ p/s/cm^2/sr), suggesting that this administration route might not be suitable for targeting a broader range of organs. Nevertheless, the SC route has been widely explored in literature for vaccination purposes, and we have shown that SC-administered LNPs loaded with Tc24 are capable of eliciting robust immune responses.[19] (iii) IP administration showed how LNPs mainly accumulated within the organs that populate the peritoneum, with the liver, spleen, lungs, and kidneys having the highest signal ($3.64 \times 10^6 \pm 1.71 \times 10^6$ p/s/cm^2/sr, $4.14 \times 10^5 \pm 2.53 \times 10^5$ p/s/cm^2/sr, $9.71 \times 10^4 \pm 8.21 \times 10^4$ p/s/cm^2/sr, and $7.79 \times 10^4 \pm 4.73 \times 10^4$ p/s/cm^2/sr, respectively). The protein expression signal followed the same trend ($3.64 \times 10^6 \pm 1.71 \times 10^6$ p/s/cm^2/sr, $4.14 \times 10^5 \pm 2.53 \times 10^5$ p/s/cm^2/sr, $9.71 \times 10^4 \pm 8.21 \times 10^4$ p/s/cm^2/sr, and $7.79 \times 10^4 \pm 4.73 \times 10^4$ p/s/cm^2/sr, respectively). Finally, (iv) IM administration gave a high signal in the injection site, followed by the one in the left lymph node proximal to the injection site ($6.15 \times 10^8 \pm 4.98 \times 10^8$ p/s/cm^2/sr for fluorescence and $1.09 \times 10^6 \pm 9.79 \times 10^5$ p/s/cm^2/sr for luminescence). Despite the absence of evident fluorescence in the liver, some protein expression was detected in the liver: this could be related to the local uptake of the LNPs within the bloodstream upon IM administration. LNPs that enter the bloodstream are quickly brought to the liver (as seen for IV administration), where hepatocytes can take up the vesicles and trigger protein translation. Histological sections of organs from these animals did not show any evidence of inflammation or acute toxicity (Figure S1a,b).

While IV administration could lead to the highest protein production, as shown by our biodistribution study, vaccines usually exploit parenteral administration for a variety of reasons that go beyond reduced training needed to perform these injections and decreased risks for infections.[31] In fact, SC and IM routes are preferred because those areas are rich in APCs and

https://doi.org/10.1021/acsami.3c18830
ACS Appl. Mater. Interfaces 2024, 16, 15832−15846

lymphatic vessels, which could potentially trigger stronger immune responses compared to IV or IP routes. Additionally, we previously demonstrated that the SC route could elicit a strong response for a monovalent Tc24 mRNA vaccine, giving us compelling evidence to support the choice of the SC route.[19]

Vaccine Efficacy: Bivalent ASP-2 + Tc24 mRNA Vaccine Reduces Parasite Burden in a Chronic CD Mouse Model. In order to assess the efficacy of our drug delivery systems for vaccine purposes, we evaluated the immunogenicity and efficacy of our mRNA-based therapeutic vaccine targets in *T. cruzi*-infected chronic mouse model of CD. Female C57BL/6J mice were infected with *T. cruzi* and, 70 days postinfection (DPI), were divided into six groups (n = 15 per group) as described in Table 1. Adopting a therapeutic vaccine strategy, animals were

Table 1. Experimental Groups[a]

group	antigen or control	antigen dose (μg)	infection
1	saline		no
2	saline		yes
3	empty LNPs		yes
4	Tc24 mRNA	10	yes
5	APS-2 mRNA	10	yes
6	Tc24 + ASP-2 mRNA	20 (10 each)	yes

[a]All mice were infected with 5000 *T. cruzi* H1 clones K68 by intraperitoneal injection. Mice received immunization subcutaneously, the prime at 70 and two boosters at days 77 and 84 DPI.

administered three doses, once a week, starting at 70 DPI, during the early chronic phase of infection, following the treatment regimen represented in Figure 1a and comparing therapeutic vaccination strategies described in Figure 1b. In detail, we wanted to compare the efficacy of a therapeutic vaccination strategy involving LNPs loaded with a single antigen or with both antigens. Hence, we collected blood, heart, and muscle tissues at 14- and 126 DPB after all animals had completed the three-dose treatment regimen. We also measured the parasite burden in the heart and skeletal muscle and parasitemia in the blood. While no change was observed for the parasite load in the heart (Figure 5a,b), a reduction in the parasite burden was observed in the skeletal muscle of the mice infected and vaccinated therapeutically with the vaccine antigens ASP-2 and Tc24 as a monovalent and bivalent vaccine at 14 DPB (Figure 5c), with significant reduction for mice vaccinated with the Tc24 antigen. At 126 DPB (Figure 5f), there was no reduction of parasite burdens in the heart or skeletal muscle. However, an overall reduction in the parasitemia was found in the animals vaccinated with the monovalent vaccine Tc24 and ASP-2, as well as the bivalent formulation Tc24 + ASP-2 at 126 DPB.

Vaccine Efficacy: Therapeutic Mono- or Bivalent Vaccination with ASP-2 and Tc24 mRNA Protects against Early Chronic Cardiac Inflammation. Clinical outcomes of CD involve cardiac complications related to parasite burden in the tissue, which triggers chronic cardiac inflammation.[32,33] Concurrently, inflammation and fibrosis can arise in the skeletal muscle. Here, a measurement of the heart and skeletal muscle cellular infiltrate at 14- and 126-DPB allowed us to evaluate whether therapeutic vaccination with the ASP-2 and Tc24 mRNAs as monovalent or bivalent vaccines protected the tissues in the mice infected with *T. cruzi*. At 14 DPB, the group immunized with the bivalent vaccine ASP-2 + Tc24 showed a lower amount of cell infiltration compared with the unvaccinated animals (control) and the mice treated with empty LNPs (Figure S2a). However, the groups vaccinated with the Tc24 mRNA or ASP-2 vaccine had no significant reduction. Additionally, the fibrosis detected in the tissues remained consistent across treatment strategies. Interestingly, both the cardiac cellular infiltration and fibrosis increased at 126 DPB (Figure S2b), suggesting that vaccination with a bivalent vaccine could have a short-term protective effect on the cardiac damage caused by infection with *T. cruzi*. No significant differences were detected in the levels of cardiac fibrosis (Figure S2c,d). Interestingly, vaccination had no effect on inflammation and fibrosis in skeletal muscle (Figure S3).

Vaccine Immunogenicity: Evaluation of Cytokines Secreted by Splenocytes. The rationale behind the use of a bivalent vaccine was to utilize surface proteins expressed in multiple stages of the parasite,[8] specifically the trypomastigote and the amastigote stages, to generate a more robust immune response capable of recognizing *T. cruzi* throughout its life cycle. Previous evaluations of these antigens as individual vaccine candidates had already yielded promising results.[12,34−43] In this study, we assessed the efficacy of our therapeutic vaccination strategy in vivo, which involved administering three doses of either the monovalent or the bivalent mRNA vaccines at 70, 77, and 84 DPI. The spleen, characterized by the presence of various leukocyte populations, including T cells, B cells, DCs, and macrophages, plays a crucial role in immune response regulation, encompassing innate and adaptive immune system responses.[6] Therefore, we conducted a cytokine release assay using splenocytes from vaccinated mice to determine the cytokines secreted upon restimulation with the vaccine antigen in a monovalent or bivalent mRNA vaccine.[44] We evaluated seven cytokines, categorized as proinflammatory (IFN-γ, TNF-α, IL-2, IL-22, and IL-6) and anti-inflammatory (IL-4 and IL-10).[45] IL-13 and IL-17A were also measured, albeit at levels below the assay's sensitivity. A successful vaccine profile is expected to yield a T-helper 1 cell (Th1-type) response, characterized by the production of the pro-inflammatory cytokines IFN-γ, TNF-α, and IL-2, which are crucial for controlling *T. cruzi* infection, involved in activating immune cells, promoting inflammation, and enhancing the generation of a specific immune response.[46,47] In detail, IFN-γ and TNF-α promote the activation of macrophages and other immune cells.

Meanwhile, IL-2 plays a role in the activation and proliferation of T cells and in maintaining the T cell memory. Finally, IL-6 is involved in B-cell activation and antibody production. Conversely, a Th2-type response characterized by the production of IL-4, IL-5, and IL-10 is associated with susceptibility to *T. cruzi* infection and the development of chronic CD.[47] However, anti-inflammatory cytokines such as IL-4, IL-10, and proinflammatory cytokine IL-22 regulate and control the immune response to vaccines, with IL-4 promoting antibody production by B cells and IL-10 suppressing excessive inflammation and preventing damage to healthy tissue. Maintaining a balance between Th1 and Th2 immune responses is essential for an effective immune response while mitigating the risks of excessive inflammation. Our results demonstrated specific immune responses in mice vaccinated with Tc24 and ASP-2 individually at 14 DPB (Figure 6a,c), with a subsequent decline in the response between 14- and 126-DPB (Figure 6b,d). Splenocytes from mice treated with monovalent vaccines restimulated with the corresponding antigens yielded high levels of proinflammatory cytokines (IFN-γ, TNF-α, IL-2, IL-22, and IL-6) and of and anti-inflammatory cytokines (IL-4 and IL-

https://doi.org/10.1021/acsami.3c18830
ACS Appl. Mater. Interfaces 2024, 16, 15832−15846

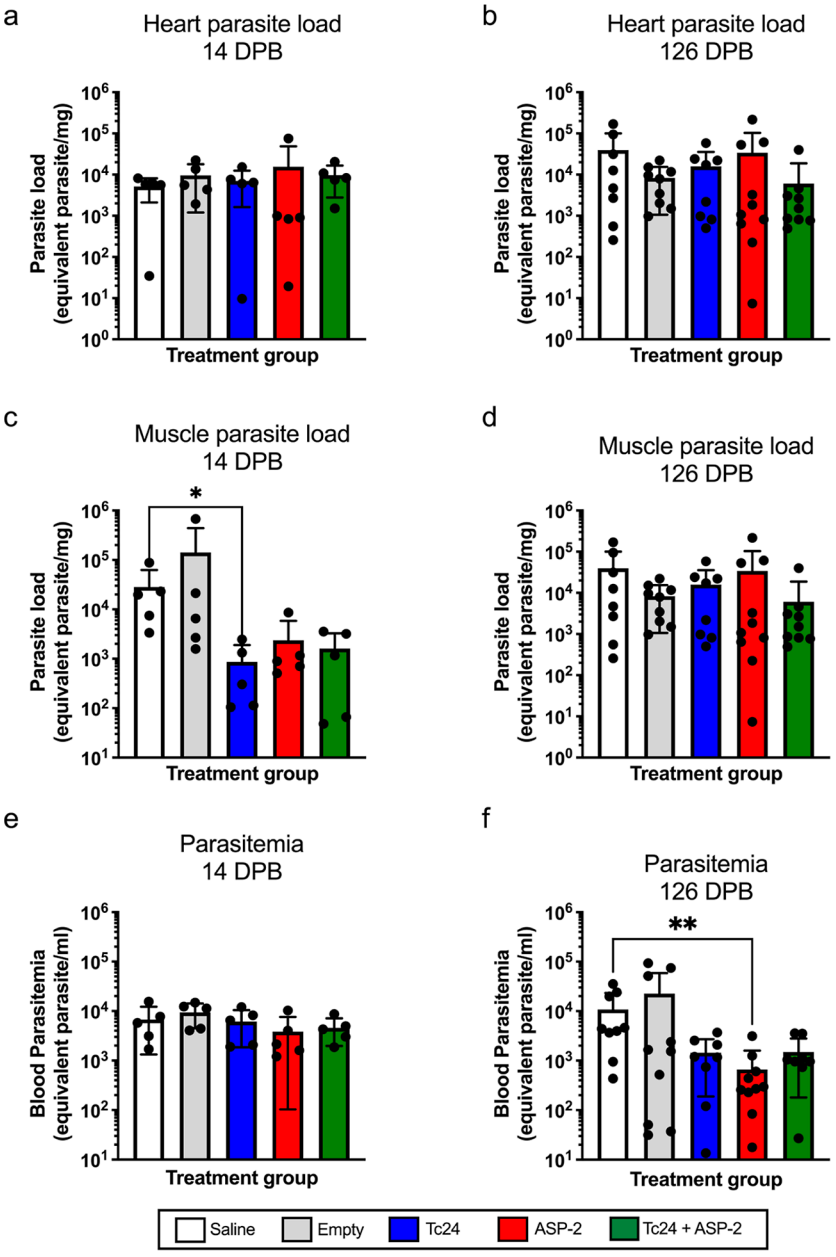

Figure 5. Bivalent ASP-2 + Tc24 mRNA vaccine reduces parasite burden. To assess the efficacy of our drug delivery systems for vaccine purposes, we tested them in vivo in a murine model of CD. After infection, mice received three doses of the mRNA vaccines on days 70, 77, and 84 postinfection, and they were sacrificed at 14- and 126-DPB. Here, we show parasite burden in (a,b) the heart; (c,d) skeletal muscle; as well as (e,f) the parasitemia. While no alteration was noted in the parasite load within the heart, a decrease in parasite burden was measured in the skeletal muscle of mice subjected to therapeutic infection and vaccination with the antigens ASP-2 and Tc24, both as monovalent and bivalent vaccines at 14DPB. Nevertheless, by 126 DPB, there was no discernible reduction in parasite burdens within the heart and skeletal muscle. However, an overall decline in parasitemia was evident in animals vaccinated with the monovalent Tc24 and ASP-2 vaccines, as well as the bivalent formulation Tc24 + ASP-2 at 126 DPB. *P*-values of $\leq$0.05, $\leq$0.01, $\leq$0.001, and $\leq$0.0001 are represented as one, two, three, and four symbol characters, respectively.

10) 14 DPB (Figures S4 and S6), only for those levels to decrease 126 DPB (Figures S5 and S7).

In contrast, mice immunized with the bivalent vaccine Tc24 and ASP-2 exhibited a specific response at 126 DPB; splenocytes restimulated with both antigens showed an increase of both proinflammatory and anti-inflammatory cytokines from 14 to 126 DPB (Figures 6e,f, S8, and S9), demonstrating the potential of a bivalent vaccination strategy in providing a more robust response. We hypothesize that the antigens Tc24 and ASP-2 became less prevalent, evading the immune response over time and posing challenges for recognition by the immune system in animals vaccinated with monovalent but not bivalent vaccines, which contain antigens for both forms of the parasite.[48] Alternatively, the induced immune response may have waned over time due to a decline in the number or quality of memory cells or a general decrease in the immune response quality.

Understanding the dynamics of mRNA vaccine-induced immune responses and their durability is crucial for optimizing vaccination strategies against CD. The immune response to the Tc24 and ASP-2 monovalent mRNA vaccines exhibited a specific cytokine secretion pattern 2 weeks after the last immunization. However, over time, the immune system's

https://doi.org/10.1021/acsami.3c18830
ACS Appl. Mater. Interfaces 2024, 16, 15832−15846

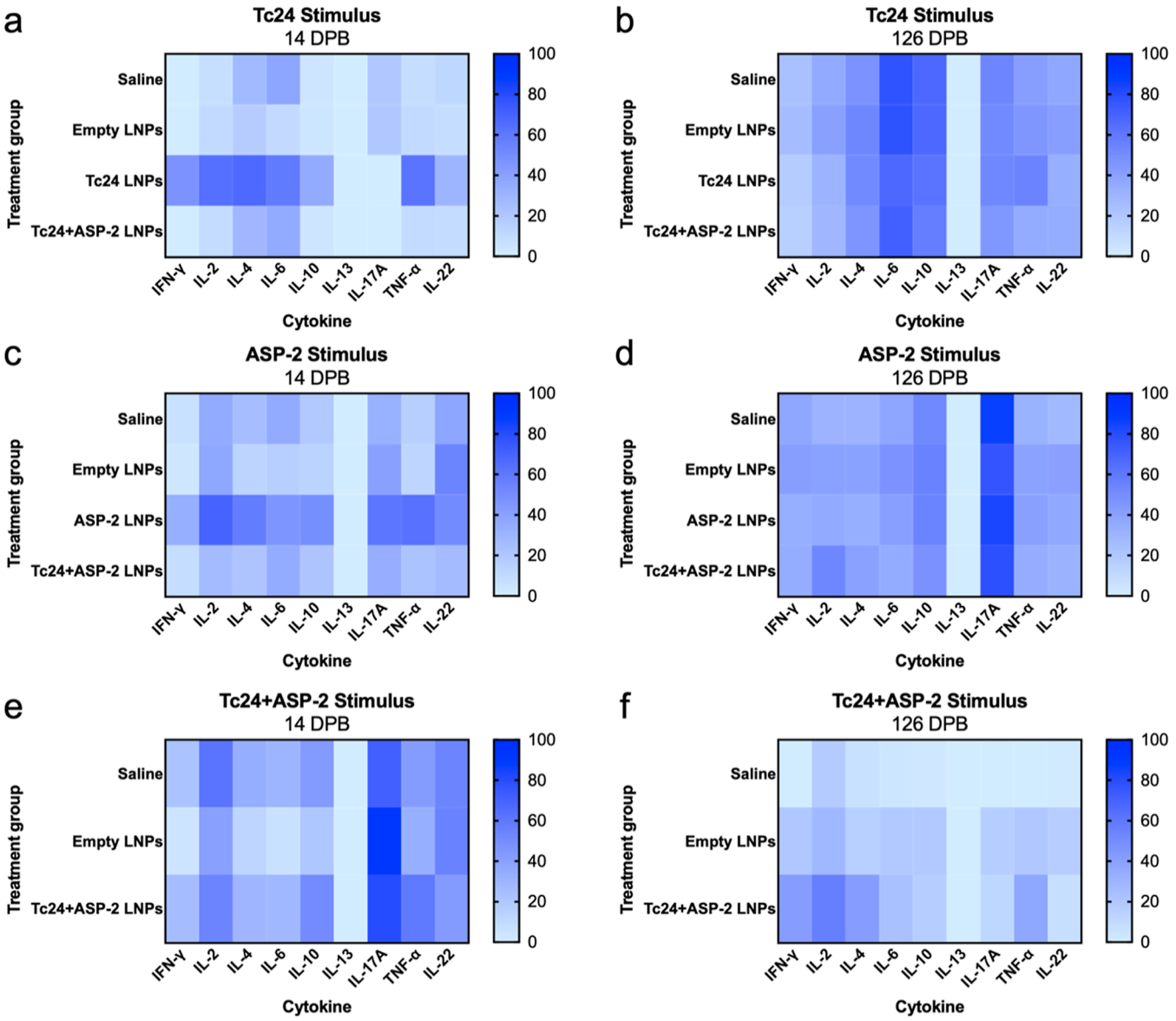

Figure 6. Evaluation of cytokines secreted by splenocytes of vaccinated mice. The spleen, characterized by various leukocyte populations, including T cells, B cells, DCs, and macrophages, plays a crucial role in immune response regulation, encompassing innate and adaptive immune system responses. Here, we conducted a cytokine release assay (Luminex) using splenocytes from vaccinated mice to determine the cytokines secreted upon restimulation with the vaccine antigen, either in a monovalent or bivalent mRNA vaccine. We evaluated nine cytokines, categorized as proinflammatory (IFN-γ, TNF-α, IL-2, IL-22, and IL-6) and anti-inflammatory (IL-4 and IL-10). IL-13 and IL-17A were also measured, albeit at levels below the assay's sensitivity. Here, we show heatmaps with normalized values for the aforementioned cytokines in splenocytes restimulated with (i) the Tc24 antigen for (a) 14 DPB and (b) 126 DPB; (ii) the ASP-2 antigen for (c) 14 DPB and (d) 126 DPB; and (iii) the combination of Tc24 + ASP-2 antigens for (e) 14 DPB and (f) 126 DPB.

response to the vaccine may have weakened or declined, leading to a loss of protection. The duration of vaccine-induced protection varies depending on factors such as the pathogen, the individual's immune system, and vaccine type. This decline in the level of protection can be attributed to a series of factors. For instance, a decrease in the number of memory cells or changes in the quality and specificity of the immune response could contribute to that outcome. In the case of the monovalent vaccine, the loss of a specific immune response at 126 DPB, 16 weeks after last immunization, could be attributed to antigenic drift or shift, which can reduce the vaccine's effectiveness, especially if the antigens no longer match the circulating strains of the parasite.[49]

CONCLUSIONS

While vaccines have successfully prevented and controlled many infectious diseases caused by bacteria and viruses, developing effective vaccines against eukaryotic parasites poses unique challenges.[50] Parasites often have large genomes and complex life cycles involving multiple developmental stages, which sometimes alternate between different hosts. Each stage may express unique antigens, making it challenging to identify suitable vaccine targets that provide broad protection across all life cycle stages. Moreover, many parasites, including *Trypanosoma*, employ antigenic variation. They can rapidly change the surface antigens they express, evading the host's immune response.[51] This requires identifying conserved antigens as vaccine targets that can trigger an immune response

https://doi.org/10.1021/acsami.3c18830
ACS Appl. Mater. Interfaces 2024, 16, 15832−15846

with the ability to overcome antigenic variation.[52] However, there is a limited understanding of the specific immune responses that are required to confer protection in many parasitic infections. Without clear correlates of protection, it is challenging to determine the efficacy of vaccine candidates during preclinical and clinical trials. Finally, logistical challenges further complicate the design of immunization campaigns, particularly when targeting remote or resource-limited areas where parasitic infections are widespread.[53,54] The delivery of vaccines to such locations presents significant obstacles and hurdles.

Despite the promise of global access and affordability, the mRNA-based vaccine technology faces significant hurdles before the ecosystem of global manufacturers can learn to adopt it: such technology is important to be assessed to build preclinical regulatory-enabling evidence of its value toward the use for preventing or treating neglected and infectious diseases of importance in the low- and middle-income countries.

Overall mRNA-based vaccines do offer many advantages, including the feasibility of manufacturing speed, scalability, long-term storage, regulatory flexibility, safety, efficacy.[55] However, their successes have mostly been restricted to preventing viral illness. One approach to expand the mRNA vaccine platform to nonviral or more complex pathogens, including eukaryotic parasites, is to consider bivalent or multivalent approaches. Multivalent vaccination approaches have also shown to have many benefits, including the possibility of increasing protection against the same or different pathogens by elucidating immune response to two or multiple antigens.[56] Moreover, when compared to the traditional therapeutic approach to CD (which involves drugs with significant side effects, Benznidazole and Nifurtimox, that prompt ∼40% of the patients to discontinue treatment), global vaccination efforts dedicated to the Covid-19 pandemic with mRNA-based technology have saved tens of millions of lives, while the spectrum of their side effects, spanning from mild reactogenicity to exceptionally rare severe illnesses, was much lower in incidence.[57]

In this work, we explored combining the use of mRNA-technology with a bivalent vaccine target approach. For the first time we assessed the production and proof-of-concept immunogenicity and efficacy study of a bivalent mRNA-based vaccine for *T. cruzi*. We assessed the homogeneity and stability of the LNP formulations, as they play a crucial role in successfully translating the platform and subsequent production and storage processes. Additionally, the toxicity, uptake, and biodistribution studies offered valuable insights into potential variations in target organs resulting from different routes of administration. These findings are particularly significant for determining the potential therapeutic effectiveness of the vaccine. The route choice depends on the vaccine's characteristics, the desired immune response, the target population, and the availability of appropriate administration methods. Each route has its considerations regarding stability, delivery efficiency, and potential side effects. It was further noted that a higher distribution of LNPs does not always correlate with a better expression of the mRNA. This can be observed from Figure 4, where the LNPs reaching the spleen did not produce a Luciferase signal as strong as in other organs (i.e., liver). Efficient spleen targeting in vaccines can improve immune responses, including increased antibody production, enhanced cellular immunity, and prolonged antigen presentation.[58,59]

Our results show promising outcomes not only in reducing the parasite burden in the chronic phase of CD but also in reducing the early cardiac damage caused by *T. cruzi* infection. We evaluated the immunogenicity and effectiveness of Tc24 and ASP-2 mRNA-based candidates, as both monovalent and bivalent vaccine strategies, employing an in vivo chronic mouse model of CD. The reduction in the cardiac parasite burdens in the mice vaccinated with bivalent vaccine Tc24 + ASP-2 suggests a synergist effect, where the presence of one antigen enhances the immune response triggered by the other, as well as an increase in the recognition of the parasite stages, boosting its elimination (ASP-2 amastigotes and Tc24—trypomastigotes and amastigotes). Finally, our results show a long-lasting effect in the bivalent group at 126 DPB but not in the monovalent groups of Tc24 mRNA or ASP-2 mRNAs alone. An added challenge in CD management is the therapeutic effect on cardiac tissue. The therapeutic goals include reductions of parasite load (amastigotes and trypomastigotes) in the heart cardiac, with simultaneous decreases in host inflammatory responses and collagen deposition leading to cardiac fibrosis. An ideal target product profile for a CD therapeutic vaccine includes all three performance features, or at the very least no exacerbation of either inflammation or fibrosis that could worsen therapeutic outcomes. While the present study represents the first proof of concept of the feasibility of using multivalent mRNA vaccination strategies for CD, there is room for improvement in different areas. For example, improving the LNP formulation and the purity of the mRNA could significantly boost the effectiveness of the treatment. Additionally, exploring different antigen dosages, as well as adding a third booster to the schedule, would provide a better picture of the potential of our mRNA-based therapeutic vaccine. Nevertheless, this is the first study demonstrating partial efficacy of a multivalent mRNA based therapeutic vaccine against CD, which induced a desirable immune response and reduced cardiac pathology. This is the first study demonstrating partial efficacy of a multivalent mRNA based therapeutic vaccine against CD, which induced a desirable immune response and reduced cardiac pathology. This shows promise for developing next generation therapeutic vaccines to improve cardiac health for CD patients, using mRNA or potentially mRNA-protein prime-boost approaches. However, we need further optimization in terms of vaccine dose, delivery, and formulation in order to achieve maximal protection and minimal cardiotoxicity.

METHODS

mRNA Production. ASP-2 and Tc24 mRNA production was assess as previously described.[19] Tc24 and ASP-2 sequences were cloned into pTNT (Promega) to facilitate mRNA transcription. To improve the ribosome binding and expression efficacy, the codon usage was optimized. A KOZAK sequence (GCCRCCAUGG) was added ahead of Tc24 and ASP-2 ORF to assist in the initiation of the translation process. The plasmid was cloned in *Escherichia coli*. Linearization is required to avoid infinite transcription around the circle. Hence, the plasmid is digested with restriction-endonuclease BAMHI. Then, the linearized plasmids were purified on MaXtract High-Density columns (Qiagen) and by precipitation in ethanol. The integrity, yield, concentration, and purity of the linearized plasmids were measured by the absorbance at 260 nm on a Nanodrop spectrophotometer. In vitro transcription of Tc24 and ASP2-encoding mRNA was executed with T7 RNA polymerase (RiboMAX Large Scale RNA Production Systems, Promega) according to the manufacturer's instructions; we replace the uridine for modified N1-methylpseudouridine-5′-triphosphate. These RNAs were purified by precipitation in ammonium acetate and capped using a ScriptCap m7G Capping System (CellScript) to enhance cell RNA stability and translation. Before

https://doi.org/10.1021/acsami.3c18830
ACS Appl. Mater. Interfaces 2024, 16, 15832−15846

use, the mRNA quality was assessed by agarose gel electrophoresis. All RNAs were stored at −80 °C until use.

LNPs Synthesis. LNPs were synthesized with the NanoAssemblr Benchtop system, which exploits a microfluidic cartridge equipped with a staggered herringbone geometry to efficiently mix organic and aqueous phases efficiently. The choice of the lipidic composition described here is rooted in the nature of LNPs: extensive literature has demonstrated that successful genetic cargo encapsulation occurs when at least 50% of the molar percentage of the lipidic composition is represented by an ionizable cationic lipid, that is, a lipid that displays a positive charge at the acidic pH of synthesis, therefore triggering complexation with the negatively charged mRNA, while losing that charge after purification (https://www.mdpi.com/2076-393X/11/3/658). Discovery of ionizable lipids has allowed great flexibility in terms of genetic cargo delivery, while maintaining a good safety profile of the formulation, thanks to the neutral charge displayed by the final drug delivery system (10.1016/j.addr.2023.115175). Addition of other "helper lipids" in the formulation (DSPC, Cholesterol, and DMG-PEG2000) is necessary to achieve proper packaging of the genetic cargo during the nanoprecipitation process (in the case of DSPC and Cholesterol) as well as proper colloidal stability (in the case of DMG-PEG2000). Here, DLin-MC3-DMA, DSPC, cholesterol, and DMG-PEG2000 (50:10.5:38:1.5 molar ratios, respectively) were dissolved in ethanol for a final lipidic concentration of 10 mM to make the organic phase. In contrast, the aqueous phase consisted of sodium acetate buffer (50 mM) at pH 4 used alone (for empty LNPs) or combined with the mRNA of interest. In detail, an N/P ratio of 5.6 was used for the following formulations (according to the construct size of 624 bases for Tc24 and 723 bases for ASP-2): (i) 300 μg of Tc24 mRNA, (ii) 300 μg of ASP-2 mRNA, or (iii) a combination of 150 μg of Tc24 and 150 μg of ASP-2 mRNAs. The following synthesis parameters were selected: the TFR was set at 9 mL/min, the FRR was 1:3 (organic: aqueous), and the initial and final waste was 100 μL. After synthesis, LNPs were dialyzed against 1× PBS overnight and then filtered with 0.22 μm syringe filters to ensure sterility and remove potential aggregates.

LNPs Characterization. Size (nm), PDI (au), and ZP (mV) were measured via DLS using Malvern Zetasizer for 28 days postsynthesis. Samples for size and PDI measurements were prepared by adding 10 μL of NPs and 990 μL 1× PBS to a semimicrovolume disposable cuvette. In comparison, samples for ZP were prepared by adding 10 μL of sample to 90 μL of 1× PBS and 900 μL of double distilled water (ddH_2O, salt concentration was lower to avoid damage to the electrodes of the ZP cuvette used for the measurement). For both size and ZP, three measures of 15 runs each were acquired and then averaged to obtain the final value for each formulation.

mRNA encapsulation efficiency (EE %) was evaluated by using the Ribogreen RNA assay. When the dye binds to nucleic acids, its fluorescence increases proportionally and can be used to detect the concentration of mRNA encapsulated in the LNPs. Due to the nature of LNPs, it is possible to see some mRNA grafted on the outer part of the vesicles: of course, this mRNA will not be functional due to exposure to the outer side of the vesicles. To remove unencapsulated mRNA (both the one released after dialysis and the one grafted outside the LNPs) from the quantification, the signal from intact LNPs was subtracted from the signal obtained from burst LNPs. LNP samples were first diluted 1:100 in 1× TE buffer, followed by 50 μL of each diluted sample added to either 50 μL of 1× TE buffer or 100 μL of 2% Triton-X in 1× TE buffer (this step ensures bursting of LNPs). RNA standard curve, ranging from 0.1 to 2.5 μg/mL, was prepared using a combination of 2% Triton-X 100 in 1× TE buffer and 1× TE buffer as the diluent. All samples were run in duplicate and incubated at 37 °C for 10 min. Ribogreen reagent was diluted 1:100 in 1× TE buffer with 100 μL added to each well. Following a 10 min incubation at room temperature, the plate was read at E_x/E_m of 480 nm/520 nm.

The stability of the encapsulated mRNA was assessed for 28 days postsynthesis. First, the RNA was extracted from LNPs by using a lithium chloride precipitation method to evaluate mRNA integrity. Briefly, 100 μL of empty or loaded LNPs were mixed with 300 μL of lithium chloride in pure ethanol (34 mg/mL solution). The solution was centrifuged at 12,000*g* for 10 min (4 °C). After the supernatant was removed, the pellet was dissolved in 500 μL of 70% ethanol in RNase-free water, and another centrifugation (12,000*g*, 10 min, 4 °C) step followed. Finally, the supernatant was removed, and the pellet was dissolved in 30 μL of RNase-free water. After measuring the RNA concentration with Nanodrop, samples were diluted to a concentration of 50 ng/μL and processed through a Bioanalyzer. Samples corresponding to RNA controls (mRNA constructs loaded within LNPs) and RNA extracted at 0, 7, 14, 21, and 28 days from LNPs were submitted to assess RNA integrity.

Cell Viability Assay and Uptake. DCs were purchased from Millipore and maintained in complete media (DMEM, 10% FBS, and 1% Pen/Strep). For cytotoxicity experiments, DCs have seeded a 96-well plate at a seeding density of 8000 cells/well. After 24 h, LNPs were resuspended in media and added to the cells at the following lipidic concentrations: 0, 12.5, 25, 50, and 100 μM (n = 8 wells for each concentration). The toxicity of NP treatment was evaluated using an MTT [3-(4,5-dimethylthiazol-2-yl)-2,5- diphenyltetrazolium] assay at 24 h according to the manufacturer's instructions. Briefly, media was aspirated and replaced with MTT resuspended in complete media at 0.5 mg/mL concentration. After 2 h, the MTT reagent was aspirated and replaced with equal volume DMSO. Following 30 min of gentle agitation at room temperature, absorbance was measured at 570 nm with an excitation wavelength of 630 nm. Cell viability (%) was calculated as follows: $(\text{absorbance}_{\text{sample}})/(\text{absorbance}_{\text{control}}) \times 100$. The optical density of each well was measured using a Spark multimode microplate reader (Tecan). For the uptake evaluation, DCs were seeded in 4-well chamber slides at a concentration of 35,000 cells/well. The following day, cells were treated with rhodamine-labeled empty LNPs (50 μM lipidic concentration): after overnight incubation, cells were washed with PBS, fixed with 4% paraformaldehyde for 10 min, and washed twice with HBSS (Hank's Balanced Salt Solution). Next, cells were stained first with 5 μg/ml WGA S-10 Alexa Fluor 488 Conjugate (Invitrogen) for 10 min at 37 °C, washed twice in HBSS, and then stained with 1 μg/mL DAPI (Abcam) for 3 min at room temperature. Images were acquired with a Keyence BZ-X800 All-in-one Fluorescence Microscope and processed using Fiji Is Just ImageJ (FIJI, version 1.53c) software.

Values for cellular uptake of LNPs were calculated as follows: uptake = number of "Rhod^+" pixels, numbers of "WFA^+" pixels, where the nominator represents the signal from LNPs that have been uptaken by DCs. In contrast, the denominator represents the area occupied by the cells.

Ethics Statement. Animal experiments related to the biodistribution of LNPs were approved by the Institutional Animal Care and Use Committee (IACUC), assurance number A4555−01, at the Houston Methodist Research Institute. Animal experiments related to vaccine efficacy were performed in full compliance with the Guide for the Care and Use of Laboratory Animals, eighth edition,[60] under a protocol approved by Baylor College of Medicine's IACUC, assurance number D16-00475.

In Vivo Biodistribution and Optimization of Administration Route. Two months old female C57BL/6J were purchased from Charles River and allowed a 72 h acclimation period in the dedicated comparative medicine program facility. Mice were administered DID-stained Luciferase-loaded LNPs (Trilink, 40 μg per mouse) using four different administration routes: (i) intravenous (IV, n = 5), (ii) subcutaneous (SC, n = 5), (iii) intraperitoneal (IP, n = 5), and (iv) intramuscular (IM, n = 5). Upon administration, mice were briefly anesthetized using 2.5% isoflurane inhalation: for (i) intravenous injection, the bloodstream was accessed via retro-orbital sinus (RO); (ii) subcutaneous injection was performed using the back of the mice; (iii) IP injection was performed accessing the lower-right quadrant of the peritoneum; (iv) IM injection was delivered in the quadriceps of the left leg. 18 h postinjection, mice were euthanized, and their organs were imaged ex vivo using the IVIS Spectrum CT equipment. The formulation composition made an immediate readout of the LNPs biodistribution and protein translation available. Organs were imaged with a sequence including a fluorescence reading (E_x/E_m = 644/663 nm) and a bioluminescence reading, able to detect the luciferase protein expression if present. If the Luciferase mRNA is successfully delivered

https://doi.org/10.1021/acsami.3c18830
ACS Appl. Mater. Interfaces 2024, 16, 15832−15846

to the cytosol by the LNPs, then mice will express the protein Luciferase (mainly in the tissues where higher LNP accumulation occurs). Luciferase's substrate, Luciferin, can be injected intraperitoneally (200 μL, solution concentration of 15 mg/mL) to cause the bioluminescence reaction to occur within 10 min from the Luciferin injection.

Toxicity Evaluation: Histology. Organs extracted from mice that were administered LNPs for biodistribution studies were harvested for histology. Following IVIS imaging, organs (heart, lungs, liver, spleen, and kidneys) were immediately transferred in 10% buffered formalin and fixed overnight at 4 °C under stirring conditions. Once fixed, organs were rinsed in ddH2O and stored in 70% ethanol until further processing. Tissues were then processed in a Shandon Excelsior ES Tissue Processor and embedded in paraffin on a Shandon HistoCenter Embedding System, using the manufacturer's standard processing and embedding protocols. Organ slides were sectioned at 20 μm thickness and stained with hematoxylin, eosin (H&E), and Masson trichrome (MTC). Toxicity was evaluated by visual inspection of the histology slides.

Parasite and Mice. Ninety female C57BL/6J mice (Jackson Laboratories), aged 5−8 weeks, were used for the vaccine efficacy studies. For infection experiments, *T. cruzi* strain H1 clone K68 was used. Trypomastigotes were obtained from the blood of infected immunodeficient male ICR-SCID mice (Taconic Biosciences), animals were injected intraperitoneally with the parasite, and trypomastigotes were isolated from blood at day 35 postinfection.

Infection and Therapeutic Vaccination Strategy. All mice were infected with 5000 blood-form trypomastigotes of *T. cruzi* H1 clone K68 by intraperitoneal injection. At 70 days postinfection (DPI), animals were randomly divided into six groups of 15 mice each (Table 1). Therapeutic vaccination started in the early chronic phase of the disease. All the mice received three immunizations subcutaneously once weekly (70, 77, and 84 DPI). The initial evaluation was 2 weeks after the final vaccination at 14 DPB (5 mice per group), and the final evaluation was at 126 DPB (10 mice per group). The mice were humanely euthanized, and their blood, heart, and skeletal muscle were collected for parasitological evaluation, and spleens were collected to measure antigen-specific immune response.

DNA Isolation. DNA was obtained using the kit PDQeX Nucleic Acid Extractor (Microgem) following the manufacturer's directions for DNA purification, "Tissues or Blood" programs. DNA was purified from 5 μL of blood and 5 mg of cardiac tissue. DNA was quantified in a Nanodrop (Thermo Scientific) and stored at −80 °C.

Parasite Burden Determination by Quantitative Real-Time PCR. qPCR was conducted with DNA from blood, skeletal muscle, and cardiac tissue, following the method described by Piron et al., 2007.[61] Briefly, qPCR Master Mix TaqMan Fast Advanced Master Mix (Life Technologies, CA, USA) was used in qPCR reactions with oligonucleotides derived from *T. cruzi* satellite DNA using the following primers and probe: primers 5′ ASTCGGCTGATCGTTTTCGA 3′ and 5′ AATTCCTCCAAGCAGCGGATA 3′, probe 5′ 6-FAM CACACACTGGACACCAA MGB 3′; Life Technologies, CA, USA. Data were normalized to glyceraldehyde-3-phosphate dehydrogenase (GAPDH) (primers 5′ CAATGTGTCCGTCGTGGATCT 3′ and 5′ GTCCTCAGTGTAGCCCAAGATG 3′, probe 5′ 6-FAM CGTGCCGCCTGGAGAAACCTGCC MGB 3′; Life Technologies, CA, USA). qPCR was performed by using a Quant Studio 3 thermocycler (Applied Biosciences). Parasite equivalents were calculated from a standard curve of known parasite numbers.

Inflammation and Fibrosis in Heart and Skeletal Muscle. Hearts and skeletal muscles harvested from mice dedicated to vaccination experiments were processed as described above. The histopathology slides images were collected with AmScope United Scope LLC, CA, USA ME580 brightfield microscope equipped with LMPLAN40-065 × 40 objective using an 18-megapixel camera at fixed upper and lower light levels. Images were analyzed using the ImageJ software (available at https://www.nih.gov/). To determine the total area of the tissue being examined, the white background was selected and then subtracted from the total pixel count in each image. For each image, a specific area of interest was selected based on the color of the staining technique used. For example, Hematoxylin & Eosin (H&E) stains cell nuclei deep blue-purple, while Masson's Trichrome (MTC) stains collagen in blue. The selected area was then divided by the total tissue area, resulting in a ratio indicating the degree of inflammation or fibrosis in the tissue.

Splenocyte Preparation. Spleens were transferred to a gentle MACS C Tube containing 3 mL of sterile PBS and homogenized on a gentle MACS Dissociator (Miltenyi Biotech). Red blood cells from the spleen homogenates were lysed with ACK lysis buffer (Lonza, 10-548E). The lysis solution was diluted 5-fold with RPMI medium supplemented with 10% fetal bovine serum FBS, 1× penicillin−streptomycin (Pen−Strep), and L-glutamine (cRPMI medium). Splenocytes were then pelleted by centrifugation for 5 min at 300*g*. Next, splenocytes were resuspended in 5 mL of cRPMI medium and passed through 40 μm strainers (BD Biosciences, 352,340). Next, cells were counted using acridine orange-propidium iodide live/dead dye and a Cellometer Auto 2000 (Nexcelom Bioscience) automated cell counter. Then, for each sample, 1×10^6 live splenocytes were incubated in a 96-well nontissue culture plate with either 10 μg/mL recombinant Tc24-C4 protein, 20 ng/mL, ASP-2 Peptide 20 ng/mL, phorbol 12-myristate 13-acetate (PMA)−1 μg/mL ionomycin, or cRPMI only for 48 h at 37 °C in 5% CO_2.[62]

Antigen-Specific Cytokines Luminex. After 48 h, the cell-free supernatant of restimulated splenocytes was collected and stored at −80 °C until use. Using a Luminex-based assay, the secreted cytokines levels of IL-2, IL-4, IL-6, IL-10, IL-13, IL-17A, IL-22, IFN-γ, and TNF-α from supernatants were quantified, as previously described.[44] The levels of IL-13 and IL-17A concentrations were below the detection limit. The values of the splenocytes restimulated from the medium-stimulated cells served as the background. They were then divided by the measurement of the same mouse's antigen-stimulated cells to obtain the fold change.

Statistical Analysis. For each parameter measured, data were plotted using GraphPad Prism 9.4.1 software (GraphPad). Treatments were compared to infected untreated controls using a Kruskal−Wallis one-way ANOVA. *P* values ≤0.05 were considered significant.

ASSOCIATED CONTENT

Supporting Information

The Supporting Information is available free of charge at https://pubs.acs.org/doi/10.1021/acsami.3c18830.

Results of histology and raw data from the Luminex assay (PDF)

AUTHOR INFORMATION

Corresponding Authors

Assaf Zinger − *Center for Musculoskeletal Regeneration, Houston Methodist Academic Institute, Houston, Texas 77030, United States; Laboratory for Bioinspired Nano Engineering and Translational Therapeutics, Department of Chemical Engineering, Technion−Israel Institute of Technology, Haifa 3200003, Israel; Cardiovascular Sciences Department and Neurosurgery Department, Houston Methodist Academic Institute, Houston, Texas 77030, United States;* orcid.org/0000-0001-7894-486X; Email: assafzinger@technion.ac.il

Francesca Taraballi − *Center for Musculoskeletal Regeneration, Houston Methodist Academic Institute, Houston, Texas 77030, United States; Orthopedics and Sports Medicine, Houston Methodist Hospital, Houston, Texas 77030, United States;* orcid.org/0000-0002-4959-1169; Email: ftaraballi2@houstonmethodist.org

Cristina Poveda − *Department of Pediatrics, Division of Tropical Medicine, Baylor College of Medicine, Houston, Texas 77030, United States; Texas Children's Hospital Center for Vaccine Development, Houston, Texas 77030, United States;* Email: cristina.poveda@bcm.edu

Authors

Chiara Mancino − *Center for Musculoskeletal Regeneration, Houston Methodist Academic Institute, Houston, Texas 77030, United States*

Jeroen Pollet − *Department of Pediatrics, Division of Tropical Medicine, Baylor College of Medicine, Houston, Texas 77030, United States; Texas Children's Hospital Center for Vaccine Development, Houston, Texas 77030, United States*

Kathryn M. Jones − *Department of Pediatrics, Division of Tropical Medicine, Baylor College of Medicine, Houston, Texas 77030, United States; Texas Children's Hospital Center for Vaccine Development, Houston, Texas 77030, United States; Department of Molecular Virology and Microbiology, Baylor College of Medicine, Houston, Texas 77030, United States;* orcid.org/0000-0001-8745-1987

Maria José Villar − *Department of Pediatrics, Division of Tropical Medicine, Baylor College of Medicine, Houston, Texas 77030, United States; Texas Children's Hospital Center for Vaccine Development, Houston, Texas 77030, United States*

Ana Carolina Leao − *Department of Pediatrics, Division of Tropical Medicine, Baylor College of Medicine, Houston, Texas 77030, United States; Texas Children's Hospital Center for Vaccine Development, Houston, Texas 77030, United States*

Rakesh Adhikari − *Department of Pediatrics, Division of Tropical Medicine, Baylor College of Medicine, Houston, Texas 77030, United States; Texas Children's Hospital Center for Vaccine Development, Houston, Texas 77030, United States*

Leroy Versteeg − *Department of Pediatrics, Division of Tropical Medicine, Baylor College of Medicine, Houston, Texas 77030, United States; Texas Children's Hospital Center for Vaccine Development, Houston, Texas 77030, United States; Cell Biology and Immunology Group, Wageningen University & Research, Wageningen 6708 PB, The Netherlands*

Rakhi Tyagi Kundu − *Department of Pediatrics, Division of Tropical Medicine, Baylor College of Medicine, Houston, Texas 77030, United States; Texas Children's Hospital Center for Vaccine Development, Houston, Texas 77030, United States*

Ulrich Strych − *Department of Pediatrics, Division of Tropical Medicine, Baylor College of Medicine, Houston, Texas 77030, United States; Texas Children's Hospital Center for Vaccine Development, Houston, Texas 77030, United States*

Federica Giordano − *Center for Musculoskeletal Regeneration, Houston Methodist Academic Institute, Houston, Texas 77030, United States*

Peter J. Hotez − *Department of Pediatrics, Division of Tropical Medicine, Baylor College of Medicine, Houston, Texas 77030, United States; Texas Children's Hospital Center for Vaccine Development, Houston, Texas 77030, United States; Department of Molecular Virology and Microbiology, Baylor College of Medicine, Houston, Texas 77030, United States; Department of Biology, Baylor University, Waco, Texas 76798, United States*

Maria Elena Bottazzi − *Department of Pediatrics, Division of Tropical Medicine, Baylor College of Medicine, Houston, Texas 77030, United States; Texas Children's Hospital Center for Vaccine Development, Houston, Texas 77030, United States; Department of Molecular Virology and Microbiology, Baylor College of Medicine, Houston, Texas 77030, United States; Department of Biology, Baylor University, Waco, Texas 76798, United States*

Complete contact information is available at: https://pubs.acs.org/10.1021/acsami.3c18830

Author Contributions

CP, KMJ, JP, PJH, US, CM, AZ, FT, and MEB conceived and designed the study. CP, CM, ACL, RA, DMN, MJV, AZ, FG, and LV conducted the experiments. RK carried out plasmid linearization and mRNA production. CM and AZ carried out LNPs formulation. CP, ACL, CM, and RA collected data. CP, KMJ, CM, AZ, and JP analyzed the data. JP and MEB provided reagents. CM, CP, ACL, KMJ, JP, US, PJH, and MEB wrote the manuscript. F.T. and C.P. senior authors contributed equally to this manuscript.

Notes

The authors declare no competing financial interest.

■ ACKNOWLEDGMENTS

This work was funded by the Robert J. Kleberg Jr. and Helen C. Kleberg Foundation (P.J.H.). In addition, this project was supported by the Human Tissue Acquisition and Pathology Core at Baylor College of Medicine with funding from the NIH (P30 CA125123), the Pathology and Histology Core at Baylor College of Medicine with funding from the NIH (P30 CA125123), and the Cytometry and Cell Sorting Core at Baylor College of Medicine with funding from the NIH (NIAID P30AI036211, NCI P30CA125123, and NCRR S10RR024574) and the assistance of Joel M. Sederstrom. Illustrations were created with Biorender.com. CryoEM data was collected at the Baylor College of Medicine CryoEM ATC, which includes equipment purchased under support of CPRIT Core Facility Award RP190602. This work was done in collaboration with the Encapsulation and Validation Core of the Houston Methodist Academic Institute, which provided the LNP encapsulation services.

■ REFERENCES

(1) Dumonteil, E.; Herrera, C. The case for the development of a Chagas disease vaccine: why? How? When? *Trop. Med. Infect. Dis* **2021**, *6* (1), 16.

(2) Lidani, K. C. F.; Andrade, F. A.; Bavia, L.; Damasceno, F. S.; Beltrame, M. H.; Messias-Reason, I. J.; Sandri, T. L. Chagas disease: from discovery to a worldwide health problem. *Front. Public Health.* **2019**, *7*, 166.

(3) Bivona, A. E.; Alberti, A. S.; Cerny, N.; Trinitario, S. N.; Malchiodi, E. L. Chagas disease vaccine design: the search for an efficient Trypanosoma cruzi immune-mediated control. *Biochim. Biophys. Acta, Mol. Basis Dis.* **2020**, *1866* (5), 165658.

(4) WHO. Comprehensive, equitable health care services for all people affected by Chagas Disease. 2021; https://www.who.int/campaigns/world-chagas-disease-day/2021, accessed March 22, 2024.

(5) Lee, B. Y.; Bacon, K. M.; Bottazzi, M. E.; Hotez, P. J. Global economic burden of Chagas disease: a computational simulation model. *Lancet Infect. Dis.* **2013**, *13* (4), 342−348.

(6) Bronte, V.; Pittet, M. J. The spleen in local and systemic regulation of immunity. *Immunity* **2013**, *39* (5), 806−818.

(7) Camargo, E. P.; Gazzinelli, R. T.; Morel, C. M.; Precioso, A. R. Why do we still have not a vaccine against Chagas disease? *Memórias do Instituto Oswaldo Cruz* **2022**, *117*, No. e200314.

(8) Rios, L. E.; Vázquez-Chagoyán, J. C.; Pacheco, A. O.; Zago, M. P.; Garg, N. J. Immunity and vaccine development efforts against Trypanosoma cruzi. *Acta Trop.* **2019**, *200*, 105168.

(9) Jones, K. M.; Mangin, E. N.; Reynolds, C. L.; Villanueva, L. E.; Cruz, J. V.; Versteeg, L.; Keegan, B.; Kendricks, A.; Pollet, J.; Gusovsky, F.; et al. Vaccine-linked chemotherapy improves cardiac structure and function in a mouse model of chronic Chagas disease. *Front. Cell. Infect. Microbiol.* **2023**, *13*, 1106315.

(10) Junqueira, C.; Caetano, B.; Bartholomeu, D. C.; Melo, M. B.; Ropert, C.; Rodrigues, M. M.; Gazzinelli, R. T. The endless race

between Trypanosoma cruzi and host immunity: lessons for and beyond Chagas disease. *Expert Rev. Mol. Med.* **2010**, *12*, No. e29.
(11) Araújo, A. F. S.; de Alencar, B. C. G.; Vasconcelos, J. R. C.; Hiyane, M. I.; Marinho, C. R.; Penido, M. L.; Boscardin, S. B.; Hoft, D. F.; Gazzinelli, R. T.; Rodrigues, M. M. CD8+-T-cell-dependent control of Trypanosoma cruzi infection in a highly susceptible mouse strain after immunization with recombinant proteins based on amastigote surface protein 2. *Infect. Immun.* **2005**, *73* (9), 6017−6025.
(12) Martinez-Campos, V.; Martinez-Vega, P.; Ramirez-Sierra, M. J.; Rosado-Vallado, M.; Seid, C. A.; Hudspeth, E. M.; Wei, J.; Liu, Z.; Kwityn, C.; Hammond, M.; et al. Expression, purification, immunogenicity, and protective efficacy of a recombinant Tc24 antigen as a vaccine against Trypanosoma cruzi infection in mice. *Vaccine* **2015**, *33* (36), 4505−4512.
(13) Matos, M. N.; Cazorla, S. I.; Bivona, A. E.; Morales, C.; Guzmán, C. A.; Malchiodi, E. L. Tc52 amino-terminal-domain DNA carried by attenuated Salmonella enterica serovar Typhimurium induces protection against a Trypanosoma cruzi lethal challenge. *Infect. Immun.* **2014**, *82* (10), 4265−4275.
(14) Bivona, A. E.; Sánchez Alberti, A.; Matos, M. N.; Cerny, N.; Cardoso, A. C.; Morales, C.; González, G.; Cazorla, S. I.; Malchiodi, E. L. Trypanosoma cruzi 80 kDa prolyl oligopeptidase (Tc80) as a novel immunogen for Chagas disease vaccine. *PLoS Neglected Trop. Dis.* **2018**, *12* (3), No. e0006384.
(15) Cazorla, S. I.; Becker, P. D.; Frank, F. M.; Ebensen, T.; Sartori, M. J.; Corral, R. S.; Malchiodi, E. L.; Guzmán, C. A. Oral vaccination with Salmonella enterica as a Cruzipain-DNA delivery system confers protective immunity against Trypanosoma cruzi. *Infect. Immun.* **2008**, *76* (1), 324−333.
(16) Cazorla, S. I.; Matos, M. N.; Cerny, N.; Ramirez, C.; Alberti, A. S.; Bivona, A. E.; Morales, C.; Guzman, C. A.; Malchiodi, E. L. Oral multicomponent DNA vaccine delivered by attenuated Salmonella elicited immunoprotection against American trypanosomiasis. *J. Infect. Dis.* **2015**, *211* (5), 698−707.
(17) Matos, M. N.; Sánchez Alberti, A.; Morales, C.; Cazorla, S. I.; Malchiodi, E. L. A prime-boost immunization with Tc52 N-terminal domain DNA and the recombinant protein expressed in Pichia pastoris protects against Trypanosoma cruzi infection. *Vaccine* **2016**, *34* (28), 3243−3251.
(18) Versteeg, L.; Almutairi, M. M.; Hotez, P. J.; Pollet, J. Enlisting the mRNA vaccine platform to combat parasitic infections. *Vaccines* **2019**, *7* (4), 122.
(19) Poveda, C.; Leão, A. C.; Mancino, C.; Taraballi, F.; Chen, Y.-L.; Adhikari, R.; Villar, M. J.; Kundu, R.; Nguyen, D. M.; Versteeg, L.; et al. Heterologous mRNA-protein vaccination with Tc24 induces a robust cellular immune response against Trypanosoma cruzi, characterized by an increased level of polyfunctional CD8+ T-cells. *Curr. Res. Immunol.* **2023**, *4*, 100066.
(20) Khurana, A.; Allawadhi, P.; Khurana, I.; Allwadhi, S.; Weiskirchen, R.; Banothu, A. K.; Chhabra, D.; Joshi, K.; Bharani, K. K. Role of nanotechnology behind the success of mRNA vaccines for COVID-19. *Nano Today* **2021**, *38*, 101142.
(21) Gote, V.; Bolla, P. K.; Kommineni, N.; Butreddy, A.; Nukala, P. K.; Palakurthi, S. S.; Khan, W. A comprehensive Review of mRNA vaccines. *Int. J. Mol. Sci.* **2023**, *24* (3), 2700.
(22) Maeki, M.; Uno, S.; Niwa, A.; Okada, Y.; Tokeshi, M. Microfluidic technologies and devices for lipid nanoparticle-based RNA delivery. *J. Controlled Release* **2022**, *344*, 80−96.
(23) Roces, C. B.; Lou, G.; Jain, N.; Abraham, S.; Thomas, A.; Halbert, G. W.; Perrie, Y. Manufacturing considerations for the development of lipid nanoparticles using microfluidics. *Pharmaceutics* **2020**, *12* (11), 1095.
(24) El-Nimr, N. A. Merits and Demerits of COVID-19 Vaccines. *J. High Inst. Public Health* **2021**, *0* (0), 1−9.
(25) Udroiu, C. M.; Mota-Babiloni, A.; Espinós-Estévez, C.; Navarro-Esbrí, J. Energy-efficient technologies for ultra-low temperature refrigeration. In *Smart and Sustainable Technology for Resilient Cities and Communities*; Springer, 2022; pp 309−322.
(26) James, E. R. *Disrupting Vaccine Logistics*; Oxford University Press, 2021; pp 211−214.
(27) Fabbrizi, M. R.; Duff, T.; Oliver, J.; Wilde, C. Advanced in vitro systems for efficacy and toxicity testing in nanomedicine. *Eur. J. Nanomed.* **2014**, *6* (3), 171−183.
(28) Akinc, A.; Maier, M. A.; Manoharan, M.; Fitzgerald, K.; Jayaraman, M.; Barros, S.; Ansell, S.; Du, X.; Hope, M. J.; Madden, T. D.; et al. The Onpattro story and the clinical translation of nanomedicines containing nucleic acid-based drugs. *Nat. Nanotechnol.* **2019**, *14* (12), 1084−1087.
(29) Hou, X.; Zaks, T.; Langer, R.; Dong, Y. Lipid nanoparticles for mRNA delivery. *Nat. Rev. Mater.* **2021**, *6* (12), 1078−1094.
(30) Fleischmann, D.; Goepferich, A. General sites of nanoparticle biodistribution as a novel opportunity for nanomedicine. *Eur. J. Pharm. Biopharm.* **2021**, *166*, 44−60.
(31) Kim, J.; Eygeris, Y.; Gupta, M.; Sahay, G. Self-assembled mRNA vaccines. *Adv. Drug Delivery Rev.* **2021**, *170*, 83−112.
(32) Morris, S.; Tanowitz, H.; Wittner, M.; Bilezikian, J. Pathophysiological insights into the cardiomyopathy of Chagas' disease. *Circulation* **1990**, *82* (6), 1900−1909.
(33) Rassi, A., Jr; Rassi, A.; Marin-Neto, J. A. Chagas heart disease: pathophysiologic mechanisms, prognostic factors and risk stratification. *Memorias do Instituto Oswaldo Cruz* **2009**, *104*, 152−158.
(34) Wizel, B.; Palmieri, M.; Mendoza, C.; Arana, B.; Sidney, J.; Sette, A.; Tarleton, R. Human infection with Trypanosoma cruzi induces parasite antigen-specific cytotoxic T lymphocyte responses. *J. Clin. Invest.* **1998**, *102* (5), 1062−1071.
(35) Boscardin, S. B.; Kinoshita, S. S.; Fujimura, A. E.; Rodrigues, M. M. Immunization with cDNA expressed by amastigotes of Trypanosoma cruzi elicits protective immune response against experimental infection. *Infect. Immun.* **2003**, *71* (5), 2744−2757.
(36) Barbosa, R. P. A.; Filho, B. G.; Santos, L. I. d.; Junior, P. A. S.; Marques, P. E.; Pereira, R. V. S.; Cara, D. C.; Bruna-Romero, O.; Rodrigues, M. M.; Gazzinelli, R. T.; et al. Vaccination using recombinants influenza and adenoviruses encoding amastigote surface protein-2 are highly effective on protection against Trypanosoma cruzi infection. *PLoS One* **2013**, *8* (4), No. e61795.
(37) Ribeiro, F. A. P.; Pontes, C.; Gazzinelli, R. T.; Romero, O.-B.; Lazzarin, M. C.; Dos Santos, J. F.; de Oliveira, F.; Pisani, L. P.; de Vasconcelos, J. R. C.; Ribeiro, D. A. Therapeutic effects of vaccine derived from amastigote surface protein-2 (ASP-2) against Chagas disease in mouse liver. *Cytokine* **2019**, *113*, 285−290.
(38) Pereira, I. R.; Vilar-Pereira, G.; Marques, V.; da Silva, A. A.; Caetano, B.; Moreira, O. C.; Machado, A. V.; Bruna-Romero, O.; Rodrigues, M. M.; Gazzinelli, R. T.; et al. A human type 5 adenovirus-based Trypanosoma cruzi therapeutic vaccine re-programs immune response and reverses chronic cardiomyopathy. *PLoS Pathog.* **2015**, *11* (1), No. e1004594.
(39) Serna, C.; Lara, J. A.; Rodrigues, S. P.; Marques, A. F.; Almeida, I. C.; Maldonado, R. A. A synthetic peptide from Trypanosoma cruzi mucin-like associated surface protein as candidate for a vaccine against Chagas disease. *Vaccine* **2014**, *32* (28), 3525−3532.
(40) Durante, I. M.; La Spina, P. E.; Carmona, S. J.; Agüero, F.; Buscaglia, C. A. High-resolution profiling of linear B-cell epitopes from mucin-associated surface proteins (MASPs) of Trypanosoma cruzi during human infections. *PLoS Neglected Trop. Dis.* **2017**, *11* (9), No. e0005986.
(41) Krautz, G. M.; Krettli, A. U.; Godsel, L. M.; Engman, D. M.; Peterson, J. D. Human antibody responses to Trypanosoma cruzi 70-kD heat-shock proteins. *Am. J. Trop. Med. Hyg.* **1998**, *58* (2), 137−143.
(42) Sanchez-Burgos, G.; Mezquita-Vega, R. G.; Escobedo-Ortegon, J.; Ramirez-Sierra, M. J.; Arjona-Torres, A.; Ouaissi, A.; Rodrigues, M. M.; Dumonteil, E. Comparative evaluation of therapeutic DNA vaccines against Trypanosoma cruzi in mice. *FEMS Immunol. Med. Microbiol.* **2007**, *50* (3), 333−341.
(43) Dumonteil, E.; Escobedo-Ortegon, J.; Reyes-Rodriguez, N.; Arjona-Torres, A.; Ramirez-Sierra, M. J. Immunotherapy of Trypanosoma cruzi infection with DNA vaccines in mice. *Infect. Immun.* **2004**, *72* (1), 46−53.

https://doi.org/10.1021/acsami.3c18830
ACS Appl. Mater. Interfaces 2024, 16, 15832−15846

(44) Versteeg, L.; Le Guezennec, X.; Zhan, B.; Liu, Z.; Angagaw, M.; Woodhouse, J. D.; Biswas, S.; Beaumier, C. M. Transferring Luminex® cytokine assays to a wall-less plate technology: Validation and comparison study with plasma and cell culture supernatants. *J. Immunol. Methods* **2017**, *440*, 74−82.
(45) Poveda, C.; Fresno, M.; Gironès, N.; Martins-Filho, O. A.; Ramírez, J. D.; Santi-Rocca, J.; Marin-Neto, J. A.; Morillo, C. A.; Rosas, F.; Guhl, F. Cytokine profiling in Chagas disease: towards understanding the association with infecting Trypanosoma cruzi discrete typing units (a BENEFIT TRIAL sub-study). *PLoS One* **2014**, *9* (3), No. e91154.
(46) Abrahamsohn, I. A.; Coffman, R. L. Trypanosoma cruzi: IL-10, TNF, IFN-γ, and IL-12 regulate innate and acquired immunity to infection. *Exp. Parasitol.* **1996**, *84* (2), 231−244.
(47) Ferragut, F.; Acevedo, G. R.; Gómez, K. A. T Cell specificity: A great challenge in chagas disease. *Front. Immunol.* **2021**, *12*, 674078.
(48) Versteeg, L.; Adhikari, R.; Poveda, C.; Villar-Mondragon, M. J.; Jones, K. M.; Hotez, P. J.; Bottazzi, M. E.; Tijhaar, E.; Pollet, J. Location and expression kinetics of Tc24 in different life stages of Trypanosoma cruzi. *PLoS Neglected Trop. Dis.* **2021**, *15* (9), No. e0009689.
(49) Yewdell, J. W. Antigenic drift: understanding COVID-19. *Immunity* **2021**, *54* (12), 2681−2687.
(50) Versteeg, L.; Almutairi, M. M.; Hotez, P. J.; Pollet, J. J. V. Enlisting the mRNA vaccine platform to combat parasitic infections. *Vaccines* **2019**, *7* (4), 122.
(51) Zhao, X.-Y.; Ewald, S. E. The molecular biology and immune control of chronic Toxoplasma gondii infection. *J. Clin. Invest.* **2020**, *130* (7), 3370−3380.
(52) Silva Pereira, S.; Jackson, A. P.; Figueiredo, L. M. Evolution of the variant surface glycoprotein family in African trypanosomes. *Trends Parasitol.* **2022**, *38* (1), 23−36.
(53) Williams, V.; Edem, B.; Calnan, M.; Otwombe, K.; Okeahalam, C. Considerations for establishing successful coronavirus disease vaccination programs in Africa. *Emerging Infect. Dis.* **2021**, *27* (8), 2009−2016.
(54) Heaton, P. M. Challenges of developing novel vaccines with particular global health importance. *Front. Immunol.* **2020**, *11*, 517290.
(55) Linares-Fernández, S.; Lacroix, C.; Exposito, J.-Y.; Verrier, B. Tailoring mRNA vaccine to balance innate/adaptive immune response. *Trends Mol. Med.* **2020**, *26* (3), 311−323.
(56) Collier, A.-r.Y.; Miller, J.; Hachmann, N. P.; McMahan, K.; Liu, J.; Bondzie, E. A.; Gallup, L.; Rowe, M.; Schonberg, E.; Thai, S. Immunogenicity of BA. 5 Bivalent mRNA Vaccine Boosters. *N. Engl. J. Med.* **2023**, *388*, 565.
(57) Lee, J.; Woodruff, M. C.; Kim, E. H.; Nam, J.-H. Knife's edge: Balancing immunogenicity and reactogenicity in mRNA vaccines. *Exp. Mol. Med.* **2023**, *55* (7), 1305−1313.
(58) Zhuang, Y.; Ma, Y.; Wang, C.; Hai, L.; Yan, C.; Zhang, Y.; Liu, F.; Cai, L. PEGylated cationic liposomes robustly augment vaccine-induced immune responses: Role of lymphatic trafficking and biodistribution. *J. Controlled Release* **2012**, *159* (1), 135−142.
(59) Pan, L.; Zhang, L.; Deng, W.; Lou, J.; Gao, X.; Lou, X.; Liu, Y.; Yao, X.; Sheng, Y.; Yan, Y.; et al. Spleen-selective co-delivery of mRNA and TLR4 agonist-loaded LNPs for synergistic immunostimulation and Th1 immune responses. *J. Controlled Release* **2023**, *357*, 133−148.
(60) National Research Council (US) Committee. *National Research Council (US) Committee for the Update of the Guide for the Care and Use of Laboratory Animals*; National Academies Press Washington: DC, USA, 2011.
(61) Piron, M.; Fisa, R.; Casamitjana, N.; López-Chejade, P.; Puig, L.; Vergés, M.; Gascón, J.; Prat, J. G. i.; Portús, M.; Sauleda, S. Development of a real-time PCR assay for Trypanosoma cruzi detection in blood samples. *Acta Trop.* **2007**, *103* (3), 195−200.
(62) Seid, C. A.; Jones, K. M.; Pollet, J.; Keegan, B.; Hudspeth, E.; Hammond, M.; Wei, J.; McAtee, C. P.; Versteeg, L.; Gutierrez, A.; et al. Cysteine mutagenesis improves the production without abrogating antigenicity of a recombinant protein vaccine candidate for human chagas disease. *Hum. Vaccines Immunother.* **2017**, *13* (3), 621−633.

https://doi.org/10.1021/acsami.3c18830
ACS Appl. Mater. Interfaces 2024, 16, 15832−15846